COMMUNICATION

Magnetic soft organogel supercapacitor electrolyte for energy storage†

Xinxian Ma, [iD] ‡*[a] Jiuzhi Wei,‡[a] Yuehua Liang,[a] Juan Zhang,[a] Enke Feng, [iD] [a] Zhenxing Fu[a] and Xinning Han*[ab]

A highly magnetic stable organogel electrolyte for supercapacitors was prepared *via* simple esterification using polyvinyl alcohol as the raw material. This organogel exhibits excellent mechanical properties: elongation (∼700%) and tensile strength (949.21 kPa), high flexibility, magnetism, and substantial specific capacitance (164.1 F g^{-1}). At a high scan rate of 50 mV^{-1}, the CV curve of this organic gel still maintains an ideal rectangle, showing high speed performance. It has broad prospects in the application of flexible electronic products.

In recent years, the application and development of flexible electronic materials have greatly improved our lives and society. With the rapid development of flexible electronic products, such as electronic watches and electronic skin, there is a need for miniaturised and flexible energy-storage devices.[1–4] Nevertheless, the conventional capacitors are usually button cells[5,6] or have a spiralwound[7] configuration, where the electrolyte, separator, electrode materials and current collector are packaged in stacked and rolled configurations. Such capacitors are large and heavy and cannot be used as flexible energy-storage devices. Therefore, the development of ultra-thin and flexible configurations for energy-storage devices has garnered significant attention.[8–10] Among various energy-storage devices, supercapacitors possess notable advantages such as long cycle life, high power density, good flexibility, small size and safety, making them an optimal choice.[11–15] The potential applications of large-scale, transparent and flexible electronic devices in touch sensors and displays have garnered significant attention.[16–18] Owing to their inherent flexibility,[19] good mechanical recovery,[20] excellent ionic conductivity and good

biocompatibility,[21] conductive gels can be used not only as suitable electrolytes for flexible supercapacitors but also in human activity detection, biomedical engineering, artificial skin and wearable electronic devices, among others. Among conductive gels, magnetic organogels are considered as promising and attractive materials because of their unique properties such as magnetic response and remote-control ability.[22] Magnetic organogels are composites made of an organogel matrix and magnetic inclusions.[23] In addition, the magnetic effect can be achieved by changing the synthesis process to produce high-quality electrode materials with specific performance and improved electrochemical energy-storage capability.[24] Metal oxide is one of the commonly used electrode materials for preparing electrolytes for supercapacitors,[25] and most metal oxides show magnetism.[26] In addition to metal oxides, there are also many metal-based materials used in supercapacitors, such as intermetallic compounds,[27] transition metal disulfides[28] and other carbon-based materials, which can exhibit various magnetic properties. A stronger and more ductile gel matrix can be obtained by adding inorganic nanoparticles to a gel.[29] This is because the nanoparticles, through specific interactions with the gel polymer chain,[30,31] can effectively enhance the elasticity of the polymer network, thereby increasing the mechanical strength of the gel. By adding different nanoparticles, different properties such as electrical conduction and magnetism can be elicited; such properties may expand the applications of stimuli-responsive gels in the future.[32] For example, Hu *et al.* prepared a magnetic flexible composite hydrogel with a tensile strength of about 140 kPa and good tensile properties (≈170%) using terpolymer composite.[33] Demire *et al.* a self-healing and stretchable PVA–nickel–borax (PNB) material for supercapacitor applications is presented, specific capacitance up to 88.79 F g^{-1}.[34] However, the preparation of magnetic gels with high mechanical strength and excellent electrochemical properties using magnetic materials is still a major challenge. It is possible to change the electrochemical performance of capacitors using magnetic materials. Thus far, such strategies have been minimally explored.

[a] *Ningxia Key Laboratory of Green Catalytic Materials and Technology, College of Chemistry and Chemical Engineering, Ningxia Normal University, Guyuan 756099, China. E-mail: maxinxian@163.com*

[b] *Ningxia Key Laboratory of Green Catalytic Materials and Technology, Ningxia Normal University, Guyuan 756099, China. E-mail: hanxinning@163.com*

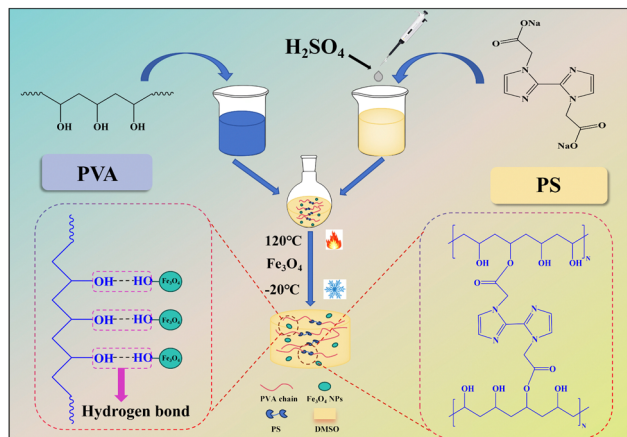‡ These authors contributed equally to this work. They should thus be considered co-first authors.

Fig. 1 Schematic diagram of the preparation of the PVA/PS/Fe$_3$O$_4$ organogel.

This paper proposes a new method for preparing a tough and adhesive magnetic organogel using polyvinyl alcohol (PVA) as a packaged system. First, superparamagnetic ferric oxide nanoparticles (Fe$_3$O$_4$ NPs) were synthesised by thermal decomposition using iron acetylacetone as the raw material (Scheme S1 and Fig. S1, ESI†).[35] Then, crosslinking agent 2,2′-(1H,1 H-[2,2′-double imidazole]-1,1′-2)sodium diacetate (PS) was synthesized using 2,2′-biimidazole (Scheme S2, ESI†). Finally, a multi-functional magnetic organogel electrolyte PVA/PS/Fe$_3$O$_4$ was prepared using PVA and PS as the raw materials (Fig. 1). PVA and PS were crosslinked and esterified at 120 °C in dimethyl sulfoxide (DMSO). After the addition of Fe$_3$O$_4$ NPs, the mechanical and electrochemical performances of the gel electrolyte improved. The viscoelastic properties of magnetic gels can be regulated, which is very useful for the development of devices with magnetic properties.

As shown in Fig. 2A, the esterification reaction between PVA and PS was explained *via* nuclear magnetic resonance (NMR) spectroscopy. Compared with the proton signal of PVA, the partial C–H proton signal of PVA/PS shifted upwards by 0.216 ppm (from 3.831 to 3.775 ppm). This was because the introduction of electron-withdrawing groups (carbonyl carbon with sp^2 hybridisation) in the PVA/PS chain weakened the electron-shielding effect of C–H. Furthermore, the signal of O–H protons in PVA split into three peaks at 4.683, 4.490 and 4.248 ppm. However, after adding PS, the splitting peak of the remaining O–H protons in PVA disappeared. After introducing the electron-withdrawing group –COOH, the O–H proton signal of PVA/PS shifted upwards to 4.393 ppm.

To further study the esterification reaction between PVA and PS, the Fourier transform infrared (FT-IR) spectra of solid PVA and the PVA/PS organogel were analysed. The FT-IR spectra of PS show typical peak areas of ν(C=O) at 1594.84 cm^{-1} (Fig. 2B). The FT-IR spectra of the PVA/PS organogel and PVA showed that PS was crosslinked with PVA due to esterification as the absorption band of ν(C=O) shifted to a higher wave number of 1708.91 cm^{-1} with the introduction of electron-withdrawing groups. Simultaneously, a typical ν(C–O–C) absorption band
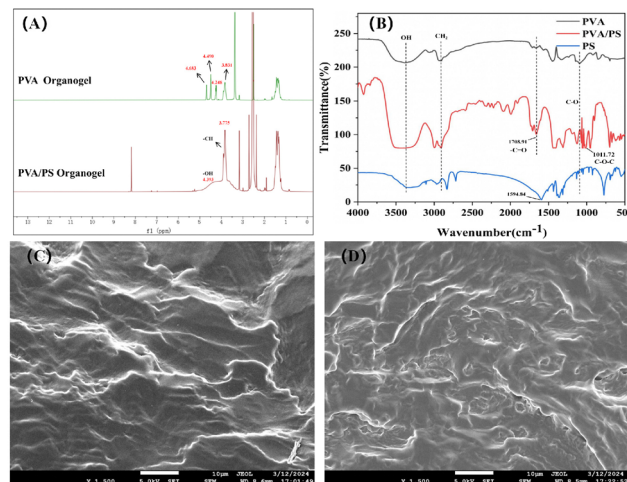

Fig. 2 (A) ^{1}H nuclear magnetic resonance (NMR) spectra of the samples. (B) Fourier transform infrared (FT-IR) spectra of the samples. (C) Scanning electron microscopy image of the PVA organogel. (D) Scanning electron microscopy image of the PVA/PS organogel.

appeared in the PVA/PS spectrum at 1011.72 cm^{-1}. The morphology of the samples was studied *via* scanning electron microscopy (SEM). The SEM image (Fig. 2C) shows the layered morphology of the PVA organogel. An appropriate amount of PS was acidified and injected into PVA, followed by esterification at 120 °C to form the PVA/PS organogel, with obvious pore structures formed in its dry form (Fig. 2D). From ^{1}H NMR, FT-IR, SEM and other data, it is evident that an esterification reaction occurred between PVA and PS.

Three types of organogels, namely PVA, PVA/PS and PVA/PS/Fe$_3$O$_4$, were prepared using the freeze–thaw method. After the shearing treatment, the mechanical properties of the organogels were tested *via* tensile tests and under artificial deformation conditions. As seen in Fig. S2 (ESI†), compared with the pure PVA organogel, the PVA/PS organogel exhibited much higher elongation ($\sim$800%), which proves that esterification crosslinking effectively changes the mechanical properties of the pure PVA organogel. Remarkably, the mechanical properties were regulated by the addition of Fe$_3$O$_4$ NPs. After Fe$_3$O$_4$ NPs were added, PVA/PS/Fe$_3$O$_4$ organogels showed significant elongation ($\sim$700%) and tensile strength (949.21 kPa) (Fig. S3, ESI†). The organogel could withstand a strain of up to 700% without any visible cracks or damage, and it could recover after stretching to almost twice its original length. Although the PVA/PS/Fe$_3$O$_4$ organogel exhibited less elongation than the PVA/PS organogel, the tensile strength of the former was much higher (322%), which greatly increased its toughness. Compared with the pure PVA organogel, the PVA/PS/Fe$_3$O$_4$ organogel had a higher elastic modulus (1.38 kPa), which was also higher than that of the PVA organogel (0.67 kPa) (Fig. S4, ESI†). These results indicate that the PVA/PS/Fe$_3$O$_4$ organogel has excellent tensile strength. In the load-bearing experiment, the PVA/PS/Fe$_3$O$_4$ organogel lifted a 2500 g reactor without showing any signs of fracture, indicating its high toughness and ability to withstand high tensile stress (Fig. 3B). Compared to other
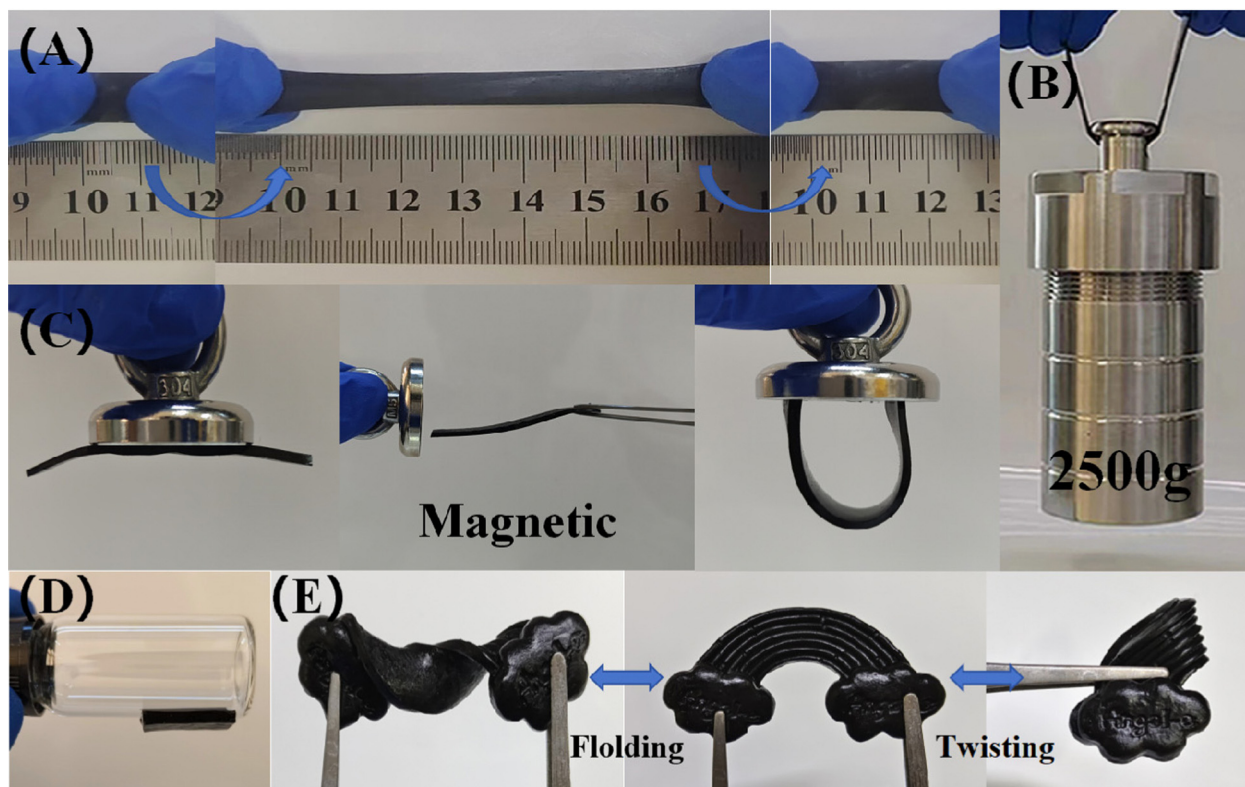
Fig. 3 (A) and (B) PVA/PS/Fe$_3$O$_4$ organogel exhibiting load-bearing capability and stretchability. (C) Magnetic response of the organogel under the action of magnets. (D) Adhesion of the organogel. (E) Deformation performance of the as-prepared organogel.

similar gels (Table 1), this organogel has excellent ensile strength and elongation. This mechanical strength is crucial for supercapacitors as they must endure internal and external stresses during repeated operations while maintaining their structure and performance. This organogel has excellent properties as an electrolyte for energy storage devices. Furthermore, Fig. 3C shows that because of the addition of Fe$_3$O$_4$, the organogel shows good magnetism, and under the action of magnetic field, it can significantly change its shape and not break. This organogel is sensitive to external magnetic fields; hence, the mechanical behaviour of the gel can be controlled through external magnetic fields.[36] This possibility lays the foundation for the wide applicability of the organogel. The organogel exhibited excellent adhesion ability towards various objects. As shown in Fig. 3D and Fig. S5(A) (ESI†), the organogel can be attached to various materials, such as iron, glass, wood, stone, plastic and agate. Therefore, the PVA/PS/Fe$_3$O$_4$ organogel electrolyte can be directly adhered to the surface of the

activated carbon (AC) electrode without auxiliary materials such as adhesive tape or packaging. In real-world applications, this substantially reduces the shedding and movement between the electrode and electrolyte layer during physical deformation, enhancing the electrochemical stability of flexible supercapacitors.[37] Fig. S5(B) (ESI†) shows that the PVA/PS/Fe$_3$O$_4$ organogel can be formed into various shapes and twisted arbitrarily (e.g. into shapes such as '2024' and 'snowflake'). Further, after the external force is removed, it can be promptly returned to almost its original shape. (Fig. 3E). Even under such large compression deformation, the gel did not crack and there was no liquid overflow, demonstrating its strong pressure resistance and water retention. Fig. S5(C) (ESI†) shows the excellent puncture resistance of the organogel. These results demonstrate the outstanding mechanical properties of the PVA/PS/Fe$_3$O$_4$ organogel, which are important for its practical applications as an electrolyte in advanced flexible energy-storage devices.

Finally, to assess the electrochemical properties of the PVA/PS/Fe$_3$O$_4$ organogel, a prototype flexible supercapacitor was fabricated using commercial AC electrodes. The electrode consisted of AC, conductive graphite and polyvinylidene fluoride (vinylidene fluoride) with a mass ratio of 8:1:1. This material was applied onto a stainless steel mesh (4 mg). Finally, the supercapacitor was assembled with a sandwich structure (Fig. S6, ESI†). Its electrochemical performance was evaluated via cyclic voltammetry (CV), electrochemical impedance spectroscopy (EIS) and constant-current charge–discharge

Table 1 Comparison of mechanical properties of organogel

Organogel	Tensile strength	Elongation (%)	Ref.
DN PVA-P(NaSS)-P(AEMA)	64 kPa	340	38
PS-p(AAm-co-MBAA) DN	0.43 MPa	590	39
PMAD/PVA/ANF	352.64 kPa	142.8	40
Fe$_3$O$_4$/PPy/PVA	575.03 kPa	—	41
PVA/PS/Fe$_3$O$_4$	949.21 kPa	691	This work
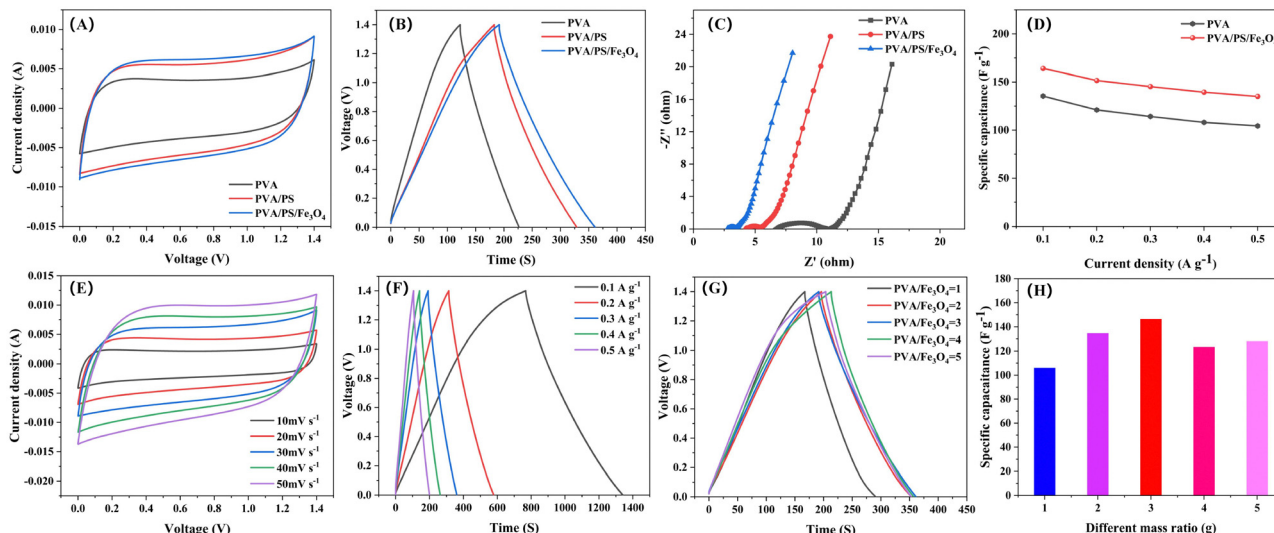
Fig. 4 (A) Cyclic voltammetry (CV) curves (30 mV s^{-1}) and (B) galvanostatic charge–discharge (GCD) curves (0.3 A g^{-1}) of the PVA, PVA/PS and PVA/PS/Fe$_3$O$_4$ organogels. (C) Electrochemical impedance spectroscopy (EIS) results of the organogel-based supercapacitor with diverse chemical compounds. (D) Relationship between the electrode specific capacitance and current density of the PVA and PVA/PS/Fe$_3$O$_4$ organogels. (E) and (F) CV and GCD curves of the PVA/PS/Fe$_3$O$_4$ organogel with a mass ratio of 3 : 1. (G) and (H) GCD curve and electrode specific capacitance of the organogels under different mass ratios at 0.3 A g^{-1}.

(GCD) tests. The CV curve of the organogel was approximately rectangular, and the GCD curve was a symmetric triangle (Fig. 4A and B), indicating typical double-layer capacitance behaviour. In addition, under identical conditions, compared with the CV curve of a capacitor with the pure PVA organogel electrolyte, that of the capacitor with the PVA/PS/Fe$_3$O$_4$ organogel electrolyte had a larger sealing area. Fig. 4C shows that in the Nyquist diagram of the organogel-based supercapacitor, there is a smaller decrease in ohmic resistance (R) because the PVA organogel slows down ion migration (6.78 Ω). However, the supercapacitors prepared with the PVA/PS/Fe$_3$O$_4$ organogel have lower ohmic resistance (2.75 Ω), possibly because xelectron transfer between Fe^{2+} and Fe^{3+} effectively increases the efficiency of ion migration. The ionic conductivities of the PVA and PVA/PS/Fe$_3$O$_4$ organogels were measured to be 7 and 18 mS cm^{-1}, respectively, indicating good ion transport characteristics. At the same current density, the specific capacitance of the PVA/PS organogel was significantly higher than that of the PVA organogel, and the specific capacitance improved further after Fe$_3$O$_4$ NPs addition with a mass ratio of 3 : 1. When the current density was 0.1 A g^{-1}, its specific capacitance reached 164.1 F g^{-1}. When the current density increased to 0.5 A g^{-1}, the specific capacitance of the PVA/PS/Fe$_3$O$_4$ organogel electrolyte reached 135.1 F g^{-1}, showing high-speed performance (Fig. 4D). The CV curve of the supercapacitor with the crosslinking agent PS exhibited a typical rectangular shape when scanned at rates of 10–50 mV^{-1} (Fig. S7, ESI†). Similarly, the CV curve of the supercapacitor based on the PVA/PS/Fe$_3$O$_4$ organogel followed a standard rectangular curve with clear symmetry and exhibited double-layer behaviour (Fig. 4E). Furthermore, the GCD curves for supercapacitors prepared using the PVA/PS organogel (Fig. S8, ESI†) and those prepared using the PVA/PS/Fe$_3$O$_4$ organogel (Fig. 4F) show the typical

triangular double-layer capacitance behaviour in the current density range of 0.1–0.5 A g^{-1}, which indicates that the organogel electrolyte has good electrochemical stability. The GCD curves and electrode specific capacitances at different mass ratios of Fe$_3$O$_4$ NPs in the supercapacitor are shown in Fig. 4G and H corresponding to operation under a current density of 0.3 A g^{-1}. The gradual increase in specific capacitance may be attributed to a decrease in the content of Fe$_3$O$_4$ NPs. Agglomeration of Fe$_3$O$_4$ NPs in the gel is reduced, and the ohmic resistance is reduced, thereby improving the charge storage capacity. We maintained the PVA/PS/Fe$_3$O$_4$ organogel at room temperature (23 °C) for 5 days to explore its weight retention. As shown in Fig. S9 (ESI†), the PVA/PS/Fe$_3$O$_4$ organogel can retain 96% of its initial weight after being kept at 23 °C for 5 days. Notably, the CV and GCD curves of supercapacitors prepared with the PVA/PS/Fe$_3$O$_4$ organogel stored for 5 days at indoor temperatures still overlap greatly with those based on the original organogel (Fig. S10 and S11, ESI†). The comparison of electrochemical properties of PVA/PS/Fe$_3$O$_4$ organogel electrolyte with those reported in other literatures is shown in Table 2.

In summary, we report a new synthesis strategy for a tough magnetic organogel electrolyte by a simple esterification reaction and addition of Fe$_3$O$_4$ NPs. This electrolyte showed excellent tensile properties, high toughness, high magnetism and large specific capacitance. The constructed carbon-based supercapacitor achieved a high specific capacitance of 164.1 F g^{-1} at a current density of 0.1 A g^{-1}. Meanwhile, the CV curve retained its perfect rectangular shape at a high scan rate of 50 mV^{-1}. This preparation approach provides new ideas for designing highly magnetic organogel electrolytes with excellent electrochemical properties.
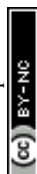
Table 2 Comparison of electrochemical properties of supercapacitors

Electrolyte	Working potential (V)	Specific capacitance (F g^{-1})	Ohmic resistance (Ω)	Ref.
PVA/glycerol/Na$_2$SO$_4$	0–2.0	54.7 (@0.5 A g^{-1})	4.9	42
B-PVA/KCl/GO	0–1.0	140 (@1 A g^{-1})	—	43
HSS-S-F/PVA	0–1.0	147 (@0.5 A g^{-1})	—	44
GPE-3/K3[Fe(CN)$_6$]	0–2.0	32.7 (@5 A g^{-1})	1.92	45
PVA/PS/Fe$_3$O$_4$	0–1.4	164.1 (@0.1 A g^{-1})	2.75	This work

Author contributions

Xinxian Ma: conceptualization, resources, funding acquisition, writing – review & editing. Jiuzhi Wei: methodology, investigation, writing – original draft. Yuehua Liang: characterize materials, performance tests. Juan Zhang, Enke Feng, Xinning Han and Zhenxing Fu: performance tests.

Data availability

The data supporting this article have been included as part of the ESI.†

Conflicts of interest

There are no conflicts to declare.

Acknowledgements

Notes and references

1 G. B. Pour, L. F. Aval and M. Mirzaee, *Recent Pat. Nanotechnol.*, 2020, **14**, 163–170.
2 L. Qing and J. Jiang, *ACS Nano*, 2023, **17**, 17122–17130.
3 P. Simon and Y. Gogotsi, *Nat. Mater.*, 2020, **19**, 1151–1163.
4 Y. Choi, M. Park, S. Kim, K. Gong, J. Wook Kim, D. Sik Kim, J. Lee, G. Jung, J. Kim, W. Yang, D.-K. Lim and J. Sook Ha, *Chem. Eng. J.*, 2024, **488**, 150931.
5 Y. Chen, L. Liu, Y. Huang, H. Cao, T. Liu, Z. Qi, J. Hu, Y. Guo, J. Sun, M. Liang, J. Wei, H. Zhang, X. Zhang and H. Wang, *Appl. Energy*, 2024, **363**, 123100.
6 Z. Qi, R. Ren, J. Hu, Y. Chen, Y. Guo, Y. Huang, J. Wei, H. Zhang, Q. Pang, X. Zhang and H. Wang, *Small*, 2024, DOI: 10.1002/smll.202400369.
7 R. Wang, D. Lei, H. Zhang, J. Liang, Z. Shang, L. Wan, Z. Li and C. Si, *Composites, Part B*, 2024, **275**, 111345.
8 X. Xue, L. Wan, W. Li, X. Tan, X. Du and Y. Tong, *Gels*, 2022, **9**, 8.
9 M. Shahid, G. M. Mustafa, A. Quader, S. M. Ramay, M. A. Shar and S. Atiq, *Diamond Relat. Mater.*, 2024, **142**, 110777.
10 Y. Wei, W. Chen, X. Ge, J. Liang, Z. Xing, Q. Zhang and Z.-X. Wang, *Polymer*, 2023, **289**, 126501.
11 K. Hu, J. Sun, Z. Guo, P. Wang, Q. Chen, M. Ma and N. Gu, *Adv. Mater.*, 2015, **27**, 2507–2514.
12 S. Cui, Y. Lv, W. Miao, W. Hou, X. Wang, Q. Hu, K. Sun, H. Peng and G. Ma, *J. Energy Storage*, 2023, **73**, 108843.
13 Q. Zhu, D. Zhao, M. Cheng, J. Zhou, K. A. Owusu, L. Mai and Y. Yu, *Adv. Energy Mater.*, 2019, **9**, DOI: 10.1002/aenm.201901081.
14 J. Chen, Y. Wang, W. Liu and Y. Ma, *ChemNanoMat*, 2019, **6**, 42–52.
15 J. Cai, X. Zhang, W. Liu, J. Huang and X. Qiu, *Polymer*, 2020, **202**, 122643.
16 X. Hu, G. Nian, X. Liang, L. Wu, T. Yin, H. Lu, S. Qu and W. Yang, *ACS Appl. Mater. Interfaces*, 2019, **11**, 10292–10300.
17 G. Bharathy and P. Raji, *J. Mater. Sci.: Mater. Electron.*, 2017, **28**, 17889–17895.
18 C. Yin, X. Liu, J. Wei, R. Tan, J. Zhou, M. Ouyang, H. Wang, S. J. Cooper, B. Wu, C. George and Q. Wang, *J. Mater. Chem. A*, 2019, **7**, 8826–8831.
19 J. Wen, B. Xu, Y. Gao, M. Li and H. Fu, *Energy Storage Mater.*, 2021, **37**, 94–122.
20 L. Ye, Q. Lv, X. Sun, Y. Liang, P. Fang, X. Yuan, M. Li, X. Zhang, X. Shang and H. Liang, *Soft Matter*, 2020, **16**, 1840–1849.
21 S. Selvam and J.-H. Yim, *J. Energy Storage*, 2023, **58**, 106340.
22 S. Kumar, F. Ahmed, N. M. Shaalan, N. Arshi, S. Dalela and K. H. Chae, *Materials*, 2023, **16**, DOI: 10.3390/ma16124328.
23 D. Carboni, B. Lasio, L. Malfatti and P. Innocenzi, *J. Sol-Gel Sci. Technol.*, 2016, **79**, 395–404.
24 Y. Zhang, Y. Wang, H. Wang, Y. Yu, Q. Zhong and Y. Zhao, *Small*, 2019, **15**, DOI: 10.1002/smll.201902198.
25 M. S. Yadav, *J. Nanopart. Res.*, 2020, **22**, DOI: 10.1007/s11051-020-05103-2.
26 A. U. Rehman, S. Nazir, R. Irshad, K. Tahir, K. U. Rehman, R. U. Islam and Z. Wahab, *J. Mol. Liq.*, 2021, **321**, 114455.
27 W. S. Leong, Q. Ji, N. Mao, Y. Han, H. Wang, A. J. Goodman, A. Vignon, C. Su, Y. Guo, P.-C. Shen, Z. Gao, D. A. Muller, W. A. Tisdale and J. Kong, *J. Am. Chem. Soc.*, 2018, **140**, 12354–12358.
28 C. Chan-Thaw and A. Villa, *Appl. Sci.*, 2018, **8**, 259.
29 J. Zhang and Z. Wang, *Catalysts*, 2022, **12**, DOI: 10.3390/catal12101096.
30 Noorjahan, S. Pathak, K. Jain and R. P. Pant, *Colloids Surf., A*, 2018, **539**, 273–279.
31 E. Kamio, T. Yasui, Y. Iida, J. P. Gong and H. Matsuyama, *Adv. Mater.*, 2017, **29**, DOI: 10.1002/adma.201704118.
32 Z. Jiang, J. Chen, L. Cui, X. Zhuang, J. Ding and X. Chen, *Small Methods*, 2018, **2**, DOI: 10.1002/smtd.201700307.
33 H. Hu, X. Zhong, S. Yang and H. Fu, *Composites, Part B*, 2020, **182**, 107623.

34 S. Demirel, R. Topkaya and K. Cicek, *J. Mater. Sci.: Mater. Electron.*, 2023, **34**, DOI: **10.1007/s10854-022-09392-2**.

35 B. Wang, C. Xu, J. Xie, Z. Yang and S. Sun, *J. Am. Chem. Soc.*, 2008, **130**, 14436–14437.

36 A. Puiggalí-Jou, I. Babeli, J. J. Roa, J. O. Zoppe, J. Garcia-Amorós, M.-P. Ginebra, C. Alemán and J. García-Torres, *ACS Appl. Mater. Interfaces*, 2021, **13**, 42486–42501.

37 X. Ma, Y. Gao, Y. Geng, J. Zhang, Y. Lai, Y. Wang, J. Tang and T. Ren, *ACS Appl. Energy Mater.*, 2022, **5**, 9303–9308.

38 A. Rahman, Solaiman, T. Foyez, M. A. B. H. Susan and A. B. Imran, *Macromol. Chem. Phys.*, 2020, **221**, DOI: **10.1002/macp.202000207**.

39 R. Wang, Z. Jiang, F. Yang, Y. Lei and J. Sheng, *Eur. Phys. J. Plus*, 2024, **139**, DOI: **10.1140/epjp/s13360-023-04817-1**.

40 W. Du, J. Zhang, Z. Zhao and X. Zhang, *Compos. Commun.*, 2020, **22**, 100438.

41 Y. Wang, Y. Zhu, Y. Xue, J. Wang, X. Li, X. Wu, Y. Qin and W. Chen, *Mater. Des.*, 2020, **193**, 108759.

42 A. G. Sánchez-Valdez, S. M. de la Parra-Arciniega, E. M. Sánchez-Cervantes and L. C. Torres-González, *J. Solid State Electrochem.*, 2023, **27**, 2917–2925.

43 H. Peng, Y. Lv, G. Wei, J. Zhou, X. Gao, K. Sun, G. Ma and Z. Lei, *J. Power Sources*, 2019, **431**, 210–219.

44 E. Cevik, S. T. Gunday, S. Akhtar, Z. H. Yamani and A. Bozkurt, *Energy Technol.*, 2019, 7, DOI: **10.1002/ente.201900511**.

45 G. Li, X. Zhang, M. Sang, X. Wang, D. Zuo, J. Xu and H. Zhang, *J. Energy Storage*, 2021, **33**, DOI: **10.1016/j.est.2020.101931**.